J. Fluid Mech. (2004), *vol.* 505, *pp.* 93–121. © 2004 Cambridge University Press
DOI: 10.1017/S0022112004008304 Printed in the United Kingdom

Particle–fluid interactions in a plane near-wall turbulent flow

By M. RIGHETTI[1] AND G. P. ROMANO[2]

[1]Department of Civil and Environmental Engineering, University of Trento, Italy
maurizio.righetti@ing.unitn.it

[2]Department of Mechanics and Aeronautics, University of Roma "La Sapienza", Italy
romano@dma.ing.uniroma1.it

(Received 30 April 2001 and in revised form 13 November 2003)

The role of particles heavier than the fluid (glass spheres in water) in a turbulent open channel flow over a smooth bed is examined at volume concentration about 10^{-3}. The present work focuses on the dynamical interaction between the solid (particles) and the fluid phases in the near-wall region. Experimental measurements have been performed by means of phase Doppler anemometry to acquire two velocity components, particle size and concentration data simultaneously; the Reynolds number of the flow was close to 15 000. It is observed that in the particle-laden flow, the vertical profiles of the streamwise mean velocity (for both fluid and solid phases) are reduced in the outer layer ($y^+ > 20$), but increased in the viscous sublayer ($y^+ < 5$) in comparison to the clear-water conditions, leading to an apparent slip kinematic boundary condition close to the wall ($y^+ \approx 2$). Moreover, in the presence of solid particles, the flow exhibits a velocity close to the wall ($y^+ < 15$) which is smaller than that of the particles, while in the outer layer the opposite takes place. In particle-laden flow, turbulence intensities of the streamwise and especially of the vertical velocity are damped for $y^+ > 10$–20 (depending on particle inertia) but enhanced in the very near-wall region ($y^+ < 5$), as is the Reynolds stress. These findings can be explained if they are referred to the mechanism of particle entrainment and deposition, which takes place close to the wall. This mechanism is related to particle inertia and to the dynamic of the structure of near-wall turbulence, which connects the buffer and outer regions with the very near-wall region. A significant momentum exchange between the two phases, which is particularly effective in the buffer region, is revealed by the quadrant analysis of the Reynolds stresses.

1. Introduction

Investigations of the effects of solid particles on near-wall turbulence have been recently performed extensively as an answer to the increasing demand for reducing wall-friction, improving sediment transport rates and increasing knowledge of particle–fluid interactions. Several theoretical, numerical and experimental studies have tried to model two-phase flows, but this is a hard task whenever particle–particle interactions have also to be taken into account (high particle concentrations). This is especially true for the near-wall region of open channel flows, where the particle concentration increases towards the bed. Early investigations, concerning sediment transport in open channel flows, accounted for particles by empirical changes of the fluid streamwise mean velocity profile (Vanoni 1946; Itakura & Kishi 1980; Coleman

https://doi.org/10.1017/S0022112004008304 Published online by Cambridge University Press

1981), while expressions for the sediment concentration were obtained by diffusive theories (e.g. Yalin 1972; Van Rijn 1989). Generally, the particle velocity is assumed substantially equivalent to the fluid velocity, except for the vertical component which is given by the fall velocity. Refined measurements in two-phase flows (Lyn 1986, 1988; Tsuji & Morikawa 1982; Tsuji, Morikawa & Shiomi 1984; Kulick, Fessler & Eaton 1994; Rashidi, Hetsroni & Banerjee 1990; Kaftori, Hetsroni & Banerjee 1995*b*; Muste & Patel 1997; Best *et al.* 1997), while confirming the modifications of the fluid mean velocity profile, also indicate a difference between particle and fluid longitudinal velocities (the particle velocity lag). Recently, expressions for such a lag have been proposed (Greimann, Muste & Holly 1999) but the hypothesis of equivalence is still retained for the r.m.s. velocity.

Moreover, the particle dynamics and the mechanisms of entrainment and deposition have been related to the dynamics of the burst–sweep cycle which characterises the near-wall turbulence (Grass 1974; Sumer & Oguz 1978; Sumer & Deigaard 1981; Rashidi *et al.* 1990). The structure of the turbulent wall layer is still an open question in the phenomenology of turbulence and much less is known about the interactions between solid particles and turbulence in this region. In particular, the mechanisms of momentum transfer between the fluid and solid phases during the entrainment and settling of particles in the wall region are not fully understood and the relevance of the experiments for the investigation of these aspects is fundamental. In the following, some results on mean velocity, r.m.s. and Reynolds stress profiles obtained by other authors are reconsidered, with the aim of highlighting some of the questions which remain.

1.1. *Mean velocity profile*

Nearly all experiments on sediment-laden flows have revealed that the fluid mean streamwise velocity is modified by the presence of particles. The results can be subdivided into two groups, according to the effect of particles on the logarithmic defect law (outer wall region) or on the logarithmic law (inner wall region). Concerning the former, Vanoni (1946) found a reduction of the von Kàrmàn 'constant', k; using a mixing length approach, this leads to a reduction of the turbulence scale and to an overall damping effect of wall turbulence. More recently, Itakura & Kishi (1980) and Coleman (1981, 1986) accounted for particles through a variation of Coles' (1956) wake-strength parameter, Π (rather than a change in k) in the logarithmic velocity defect law. The variation is still contradictory; Coleman (1986), Cellino & Graf (1999) and Graf & Cellino (1999) found an increment of Π with particle concentration, while Lyn (1986) and Valiani (1991) observed the opposite. Regarding the extent of the modified region, Lyn (1988) and Valiani (1991) found large deviations only in the wall region where the particle concentration is higher; therefore, the problem once again involves modifications in the inner wall region.

Concerning the layer closer to the wall, it should be noted that while the dimensionless defect profile is independent of the bed roughness, the profile using inner (or wall) variables strongly depends on it. In the smooth bed regime, Kulick *et al.* (1994) and Kaftori, Hetsroni & Banerjee (1995*a*, *b*) found no meaningful variation between clear water (no sediment) and sediment laden velocity profiles. On the other hand, for sediment-laden flows, Coleman (1986), Lyn (1988) (in the smooth bed regime) and Best *et al.* (1997), Muste & Patel (1997) (in the transitional bed roughness regime) have observed a decrease of the whole fluid velocity profile in comparison to clear water conditions. Coleman (1986) tried to explain such a reduction using two mechanisms;

https://doi.org/10.1017/S0022112004008304 Published online by Cambridge University Press

one due to *boundary roughness* and the other to *suspended sediments*, while Best *et al.* (1997) and Muste & Patel (1997) ascribed the velocity reduction only to the former.

Several remarks can be made about these results and these will be detailed here and in the following subsections. The first is that, for a smooth bed, one possible effect of particles is to introduce an equivalent wall roughness of the same order of magnitude as the dimensionless diameter of the particles $d_p^+ (d_p^+ = d_p u^*/\nu_f$, where d_p is the particle diameter, the subscripts p and f denote particle and fluid respectively, u^* is the friction velocity $(=(\tau_0/\rho_f)^{1/2}$, where τ_0 is the wall shear stress and ρ is the density), ν_f is the kinematic viscosity and the superscript + indicates dimensionless wall variables). However, in the measurements over a rough wall at low particle concentration (such as those by Best *et al.* 1997 and Muste & Patel 1997), it appears difficult to explain the observed downward shift of the velocity profile only through an enhancement in wall roughness. This suggests the existence of another mechanism of interaction, which could be related to the momentum exchange between the solid and the fluid during the particle settling and suspension.

One of the aims of this paper is to deeper insight into this possibility and to obtain information about the kinematics of sediment-laden flows with particular attention to the wall region. Indeed, among the aforementioned measurements, only those by Kaftori *et al.* (1995*a*, *b*) and by Kulick *et al.* (1994) were performed at a wall distance less than 40 wall units. The former used particles slightly heavier than the fluid (relative density $\rho_p/\rho_f = 1.05$), whereas the latter used heavy particles in a vertical channel. These set-ups could mask the near-wall behaviour due to the fact that the relative density and the alignment of the gravitational acceleration to the mean flow are two crucial parameters which significantly affect the particle–fluid dynamics (Tsuji & Morikawa 1982; Tsuji *et al.* 1984).

1.2. *Differences between particles and fluid mean velocities*

As already reported, experiments indicated a difference between the streamwise velocities of particles and fluid (see also Bouvard & Petkovic 1985; Rashidi *et al.* 1990; Niño & Garcia 1996); they all agree in detecting the fluid to be faster than the particles in the outer wall region. Similar results were obtained in direct numerical simulations by Pedinotti, Mariotti & Banerjee (1992). However, as pointed out, only a few data are available close to the wall ($y^+ < 40$, where y is the wall distance) to determine whether the previous result is valid in this region. Kaftori *et al.* (1995*a*, *b*) measured particle velocities higher than the fluid for $y^+ < 10$ and explain this as dependent on the probe size, which also measures the particle angular velocity. Kulick *et al.* (1994) related the particle–fluid velocity differences to the particle inertia: "high speed particles retain their momentum when moving toward the wall and rebounding from it". Greimann *et al.* (1999) derive an analytical solution for the lag velocity in the very low Stokes number regime; such a velocity approaches the fall velocity towards the bed and decreases to zero at the free surface.

It is still unclear how this difference between streamwise velocities depends on the particle size, on the distance from the wall and how this is connected to the wall dynamics.

1.3. *Velocity fluctuations*

Experimental data obtained in the last two decades have shown that particles can also affect the turbulence, damping or enhancing velocity fluctuations. One of the first theoretical investigations was made by Owen (1969) who defined the particle relaxation time ($t^* = \rho_p d_p^2/18\rho_f \nu_f$, according to Stokes' law), and suggested that small

https://doi.org/10.1017/S0022112004008304 Published online by Cambridge University Press

particles, which have a relaxation time smaller than the characteristic time of energy-containing eddies ($t_e = l/\sigma_u$, where l is the integral length scale, which is proportional to the distance from the wall and σ_u is the measured turbulence intensity at the same distance), follow the flow with some delay which causes damping of turbulent fluctuations. Gore & Crowe (1989) noted that fluctuations depend on the ratio between the particle diameter and the turbulence integral length scale; particles with $d_p/l < 0.1$ reduce flow turbulence, whereas larger particles increase it. In air flows Tsuji & Morikawa (1982) observed that the small particles (diameter 200 μm) damped the streamwise turbulence intensity outside the viscous sublayer, while the larger ones (diameter 3–4 mm) enhanced it. Kulick *et al.* (1994) noted also damping of the vertical velocity fluctuations, while Kaftori *et al.* (1995*b*), comparing the turbulence intensity of clear water and particles, observed the latter to be higher than the former at the wall and the difference to increase with the particle size. Best *et al.* (1997) confirmed the increase of turbulent fluctuations of the solid phase (of both longitudinal and vertical components) near the wall ($y/h < 0.2$–0.3), while observing damping in the outer layer.

Even though there is an agreement between the different authors as far as the logarithmic region is concerned, the behaviour for $y^+ < 10$ remains unclear, as also does the dependence on the particle concentration and size. Another open question is related to the effect of the gravitational force, which could affect fluctuations in the vertical direction because of the additional force required to suspend the particles. An inspection of the data in the literature suggests that in vertical channels (streamwise gravitational force) the vertical velocity fluctuations are not modified as much as in horizontal channels (Tsuji & Morikawa 1982; Tsuji *et al.* 1984; Niño & Garcia 1996).

1.4. *Reynolds stress and near-wall turbulence*

The behaviour of solid particles in the wall region of a turbulent flow can also be studied with regard to the dynamics of the near-wall organized structures; it is well-known that near-wall turbulent flows are arranged into alternating streaks of high- and low-momentum fluid, which evolve into characteristic vortical structures. The dynamics of this phenomenon is still a matter of debate (Kline *et al.* 1967; Kim, Kline & Reynolds 1971; Hussain 1986); it is also widely recognized that such structures interact intermittently with the outer flow through strong quasi-periodic events, consisting of ejections of low-speed fluid from the wall (grouped in a 'burst') and injections of high-speed fluid towards the wall ('sweeps') (Robinson 1991). It was also established that bursts and sweeps are the major contributors to the Reynolds stress and that bursts are responsible for the major part of the turbulent energy production and transport (Kim *et al.* 1971; Lu & Willmarth 1973). The recent hairpin model by Adrian, Meinhart & Tomkins (2000) clarifies some aspect of the re-generation mechanisms of near-wall vortical structures.

Concerning the presence of solid particles, Owen (1969) argued that sweeps are responsible for particle deposition, while Lumley (1978) proposed the ejection phenomena as candidates for the lifting up of particles from the wall. Several experiments and numerical simulations have investigated the relation between particle lifting and the bursting phenomenon (Grass 1974; Sumer & Oguz 1978; Sumer & Deigaard 1981; Pedinotti *et al.* 1992; Kaftori *et al.* 1995*a*, *b*; Niño & Garcia 1996; Shen & Lemmin 1999). The main conclusions of this huge amount of work are that the bursting process is effective in entraining particles (giving rise to fluctuations of the local concentration in phase with the burst–sweep cycle, as reported by Shen & Lemmin 1999) and that, due to the streaky structure, particles with density higher than the fluid tend to

https://doi.org/10.1017/S0022112004008304 Published online by Cambridge University Press

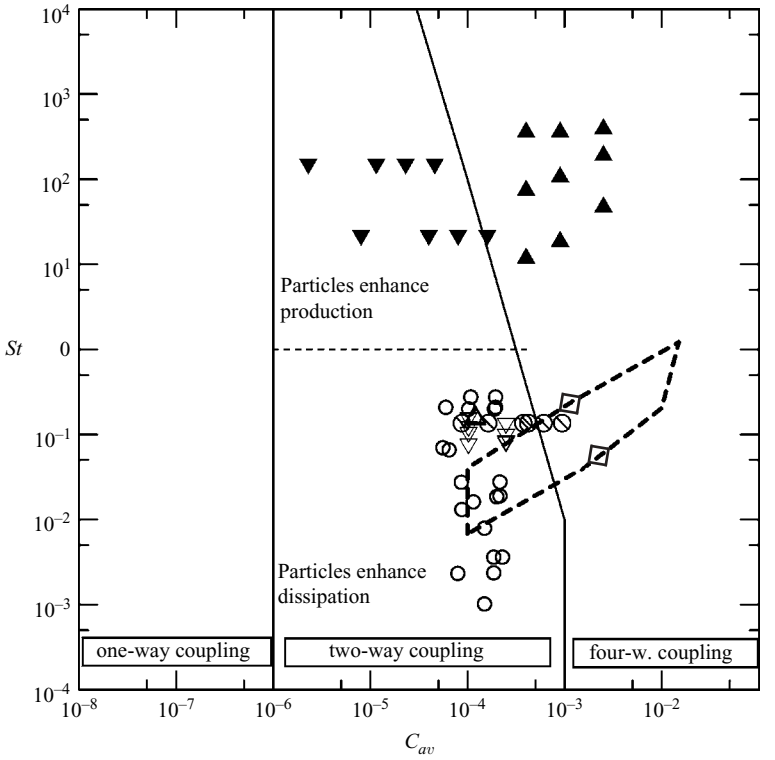


FIGURE 1. The Elgobashi (1994) classification of particle–fluid interactions. The heavy dashed lines bound the region where the present measurements are performed (moving from near-wall locations to the centreline): □, present measurements (average values for 100 μm (lower symbol) and 200 μm (upper symbol)); △, Muste & Patel (1997); ▽, Best *et al.* (1997); ⦸, Cellino & Graf (1999); ○, Kaftori *et al.* (1995*a*, *b*); ▲, Tsuji & Morikawa (1982); ▼, Kulick *et al.* (1994).

accumulate in low-speed, low-vorticity and high-strain-rate regions. This last observation is much more evident when particles with dimensionless relaxation time (in wall units) lower than about three are used (Pedinotti *et al.* 1992; Kaftori *et al.* 1995*b*; Niño & Garcia 1996). However, further quantitative details on the contributions of solid particles to the wall dynamics are still to be determined; the dynamical interaction (momentum exchange) between the two phases during the burst–sweep cycle and the effect of particle size and concentration must be also investigated.

1.5. *Classification and aim of the present work*

Some of the previous data can be summarized on a diagram containing information on particle–fluid interactions and on particle concentration. Elgobashi (1994) classified particle-laden flows using the Stokes number $St\,(=t^*/t_e$, i.e. the previously defined particle relaxation time and the characteristic time of energy-containing eddies) and the average volumetric particle concentration. This diagram is given in figure 1 for some experimental data of different authors (open symbols are used for measurements in water and filled symbols for those in air). Referring to figure 1, it is noted that, when the concentration is high enough for two-way coupling (i.e. the regime in which the particles and fluid interact and the fluid itself is significantly affected by the particles, with a significant momentum transfer between the two phases) and $St < 1$, particles enhance the dissipation of turbulent energy. At the same concentration, for larger

https://doi.org/10.1017/S0022112004008304 Published online by Cambridge University Press

Stokes numbers, vortex-shedding phenomena around particles take place, resulting in enhanced production of turbulent energy. The majority of the previous experiments in water were limited to concentration in the order of 10^{-4}. Higher concentrations were obtained in air, but in this case the particle relaxation time is much higher than the eddy turnover time (so particles are almost insensitive to fluid velocity changes).

The present measurements are performed in water with an average volumetric concentration equal to 10^{-3}, one order of magnitude larger than in the past. It should be also considered that, in near-wall flows, length and time scales of eddies decrease on approaching the wall, while concentrations of solid particles increases: therefore, on approaching the wall, the measurements move from the lower left part into the upper right part of the diagram. As a consequence, the particle–fluid interaction changes from the dissipation-enhancing to the production-enhancing regime. The heavy dashed lines in figure 1 bound this region for the present measurements; on the average, the present experimental conditions are situated at the border between the two- and four-way coupling (i.e. the regime in which the particles and fluid interact, the fluid itself is significantly affected by the particles and also particles interact among themselves), so that particle–particle interactions cannot be considered as fully dominant. It should be emphasized that the minimum distance from the wall in the present measurements is 3 wall units. Therefore, it is possible also to depict the very near-wall behaviour that was not investigated extensively in the past.

In this paper, experiments are performed on particle–fluid interactions in the near-wall region of an open channel water flow. Measurements are taken using small glass particles (size from 100 to 200 μm) at a Reynolds number ranging between about 13 000 and 14 500 and at different distances from the wall. The experimental technique used is phase Doppler anemometry, which allows separation of fluid and particle velocities and so the evaluation of the velocity differences between the phases. The aim of the paper is to clarify some of the open questions described in the previous paragraphs by investigating the modifications of the velocity field due to the presence of solid particles, especially in the near-wall region. The paper is organized as follows: the set-up and the main parameters of the experiments are described § 2; the preliminary measurements in clear water and the comparison with the results from other authors are presented in § 3; the results of measurements with solid particles and the comparison with those in clear water as well as comments are given in § 4 and concluding remarks end the paper.

2. Experimental set-up

2.1. *The facility*

A closed-circuit rectangular Plexiglas open channel is used with the axes aligned along the streamwise (x), vertical (y) and spanwise (z) directions. The channel dimensions are 3 m along x, 0.1 m along z with a free surface height, h, equal to about 0.02 m (figure 2). Experiments were performed both for clear water and for particle-laden flows; the test section was located at about 2.0 m downstream of the inlet section ($x/h \approx 100$, where $x = 0$ at the inlet). The circuit is a lengthened version of the one used by Cioffi & Gallerano (1991), without the fixed bed of solid particles (high particle concentration in a movable and erodible bed). Distilled water was used as the carrier phase seeded with polymer particles as tracers (mean diameter 12 μm, density 1.05 g cm^{-3}), whereas two glass spherical particle sizes (mean diameter 100 and 200 μm, density 2.6 g cm^{-3}) were used as the solid phase. The refractive index is the same for both the glass and the polymer particles. The average volumetric particle

https://doi.org/10.1017/S0022112004008304 Published online by Cambridge University Press

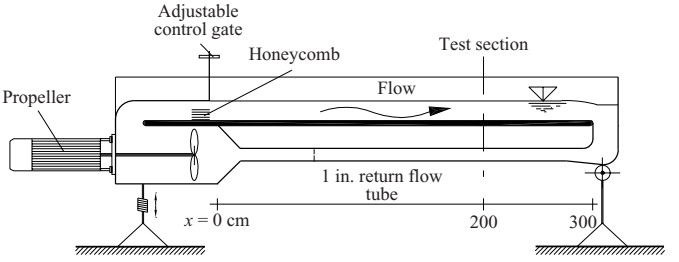


FIGURE 2. The experimental set-up.

concentration (C_{av}) in sediment-laden flow was evaluated by weighing particles and water; it was in the order of 10^{-3}. Profiles of the vertical distribution of the solid particle concentration have been measured for the two size classes (not shown); the experimental data follow reasonably well the Rousean distribution and this could be an indication that the suspended particles are in equilibrium conditions (Vanoni 1946).

The flow rate was controlled by means of a plastic propeller with variable rotation speed, thus allowing circulation of the fluid–solid mixture without damaging the glass particles. To set the initial flow depth equal to the expected uniform flow, a deflecting flow element of adjustable height was used at the inlet. Here, the flow passes through honeycombs to break up the large eddies and to obtain a fully developed turbulent uniform flow (this was verified by a preliminary analysis of the velocity field in clear-water conditions). The channel is inclined by a traversing mechanism which allows the channel slope, i_f, to be fixed between 0% and 5% with an error of $\pm 0.05\%$ (the effective slope measured with the 100 and 200 μm particles was respectively about 0.70% and 1.15%); this slope was measured at rest by means of water level staffs at four sections along x and at three locations along z in each section. The effect of this small slope on the measurements (especially on the streamwise particle velocity) is expected to be negligible. At the same locations, the flow depth was measured during each experiment to verify uniform flow conditions. The temperature was monitored during the experiments; the variation never exceeded 1.5 °C.

2.2. *The optical and signal processing systems*

The measurement system consists of a phase Doppler anemometer (PDA), which employs the green and blue light of a 2 W laser scattered from the tracers. The optical configuration was in forward-side scatter mode with a measurement volume size equal to (0.14 mm × 0.14 mm × 7.0 mm), which represents the inverse of the spatial resolution of the system, and a fringe spacing equal to 5.9 μm; a maximum and minimum fringe count was selected to further increase the spatial resolution. In comparison to the set-up of Cioffi & Gallerano (1991), the present transmitter and receiving optics configuration combined with the lower particle concentration (which enables the PDA to work with almost one particle in the measurement volume, i.e. the optimal condition) allows measurements to be performed at a very small distance from the wall (down to $y^+ \approx 2$–3).

The PDA enables one to obtain both the velocity (like the usual laser Doppler anemometry (LDA) system) and the size of particles from the phase difference of the Doppler signals between photo-receivers placed at different positions (Durst, Melling & Whitelaw 1976; Buchhave, George & Lumley 1979; Saffman & Buchhave 1984; Alimonti, Cenedese & Cioffi 1988; Cioffi & Gallerano 1991). The use of distilled water ensured that small impurities in the flow were not detected; the acquired

https://doi.org/10.1017/S0022112004008304 Published online by Cambridge University Press

Flow depth (cm)	Kinematic viscosity $(m^2\,s^{-1}) \times 10^6$	Mean velocity $(cm\,s^{-1})$	Reynolds number Uh/ν_f	Froude number $U/(gh)^{0.5}$
2.3	0.85	63	14 500	1.30

TABLE 1. Experimental parameters for clear-water conditions.

signals were due either to the polymer or to the glass particles. Before the measurements were performed, the optical configuration (i.e. location of the receiving optics, beam separation, axis inclination, focal length and laser power) was optimized by using a numerical simulation of the optical system based on Mie scattering theory (Durst *et al.* 1976; Cenedese, Cioffi & Romano 1989). The PDA technique was preferred to techniques based on the amplitude of the signal, which might mismatch small particles crossing the measurement volume close to the centre with large particles in the outer part of the volume. The average measurement errors for velocity, size and concentration are 0.5%, 3% and 10% respectively. The error in the velocity, as in typical LDA systems, depends on the measurement of the Doppler frequency, which is quite accurate. On the other hand, the error in the particle size derives from the phase measurement, which exhibits several oscillations depending on the exact receiving optics position, shape and size; simulations of the optical system lead to evaluating an average error equal to about 3% (Cenedese *et al.* 1989). The measurement of the concentration is performed by counting of the number of particles crossing the measurement volume in time (data rate); in this case, the error is larger than the previous ones due to the ambiguities in determining the effective cross-section of the measurement volume when very close to the wall (Saffman & Buchhave 1984; Alimonti *et al.* 1987).

For each experiment, the size, and streamwise and vertical velocity components of both glass (solid phase) and tracer particles (fluid phase) were simultaneously measured along the vertical axis of symmetry of the measuring cross-section in more than 30 non-equally spaced locations across the flow depth. The set-up allows the whole channel to be traversed vertically (with a resolution of 0.05 mm) so that the optics need be only slightly re-optimized at each position. At each location, the first two moments and the Reynolds stress of the streamwise and vertical velocity components are computed by averaging over about 20 000 samples (the average data sampling rate is equal to 100 Hz). The discrimination between the solid and the fluid velocity signals was made by means of the measure of the particle size; an example of such an operation is given in figure 3.

2.3. *The experiments*

The experiments were conducted in uniform flow conditions, at Reynolds numbers $Re_h = U_f h/\nu_f$ (where U_f is the depth-average streamwise flow velocity) ranging from 13 000 up to 14 500. For each experiment, the flow depth ranges from 2 to 2.3 cm, thus the width to depth ratio is quasi-constant, ranging from 4.3 to 5. It is important to point out that all the experiments were performed with Froude numbers larger than 1 (supercritical regimes). These conditions were selected after observing that for the sediment-laden experiments when moving from the subcritical to the supercritical regime the bed forms change from dunes to a plane bed configuration (without bed forms) (e.g. Yalin 1972).

The experimental conditions for the clear-water acquisitions are summarized in table 1. The data acquired in these conditions were compared to those found in the

https://doi.org/10.1017/S0022112004008304 Published online by Cambridge University Press

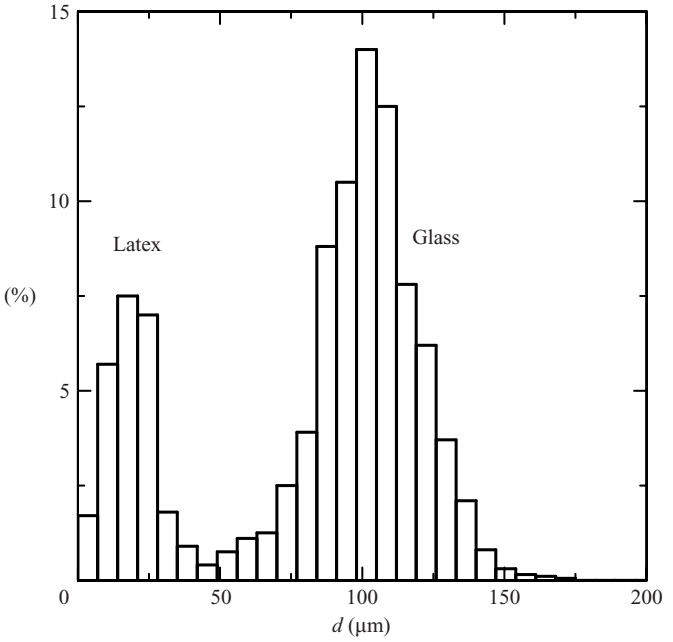


FIGURE 3. Probability density functions of the particle diameters.

	$d_p^+ = 3.8$	$d_p^+ = 8.5$
Flow depth h (cm)	2.3	2.0
Kinematic viscosity ($m^2\,s^{-1}$) $\times 10^6$	0.90	0.94
Mean velocity ($cm\,s^{-1}$)	57	60
Reynolds number Uh/ν_f	14 500	12 900
Froude number $U/(gh)^{0.5}$	1.18	1.37
Particle size d_p (μm)	100	200
Average volumetric concentration C_{av} ($\times 10^3$)	1.6	1.2
Relative density ρ_p/ρ_f	2.6	2.6
Stokes vel./friction vel. $w_s/u^* = g(\rho_p - \rho_f)/18u^*\mu d_p^2$	0.32	0.92
Max. part. Reynolds number $(U_f - U_p)_{max} d_p/\nu_f$	4.0	12
Relaxation time $t^*(\times 10^3)$ (s)	1.6	6.1
$t^{*+} = t^* u^{*2}/\nu_f$	2.04	11.3

TABLE 2. Experimental parameters for the sediment-laden conditions.

literature, to verify the suitability of the experimental set-up and of the data analysis procedure.

For each experiment in sediment-laden conditions, the average volumetric concentration is between 1.2×10^{-3} and 1.6×10^{-3}; the bed is only partially covered by the solid particles. This fact strengthens the opportunity to compare the sediment-laden flow with the clear water on a smooth rather than on a rough wall; therefore, the origin of the vertical axis (y) is taken exactly at the wall for all the experiments (clear-water and particle-laden experiments). The main features of sediment-laden acquisitions are given in table 2. The particles are heavier than the fluid and have a size much smaller than the integral scale of the flow (about 1 cm). The non-dimensional particle sizes are also smaller than 10 wall units and the particle time scale is equal to the eddy

https://doi.org/10.1017/S0022112004008304 Published online by Cambridge University Press

	Friction velocity by the momentum balance, (2) ($\mathrm{cm\,s^{-1}}$)	Friction velocity by the Reynolds stress profile, (3) ($\mathrm{cm\,s^{-1}}$)
Clear water	3.10	3.07
100 μm particles	3.40	3.09
200 μm particles	4.15	3.45

TABLE 3. Evaluation of friction velocity.

turnover time at $y^+ \approx 20$. The Stokes velocity is of the order of the friction velocity (see next section for the determination of such a velocity).

2.4. *Determination of the friction velocity*

All the results will be presented in a non-dimensional form by using wall variables. The evaluation of the friction velocity (that is the shear at the wall) is one of the crucial problems in near-wall flow measurements. As pointed out by Muste & Patel (1997), small variations of it strongly affect the plot of the mean velocity. Therefore, special care is given to determine this velocity.

The uncertainty in friction velocity depends on the evaluation method used; two possibilities have been considered (the logarithmic law was not used because in a two-phase flow the value of the von Kármán constant could be *a priori* unknown):

(i) to compute the wall shear from the momentum balance equation

$$\tau_0 = \gamma_f \left[(1 - C_{av}) + \frac{\rho_p}{\rho_f} C_{av} \right] R_h i_f \tag{2}$$

where $\gamma_f = \rho_f g$ (g is the gravitational acceleration), R_h is the hydraulic radius and i_f is the channel slope;

(ii) in analogy with the method proposed by Harder & Tiederman (1991), to compute the wall shear by the Reynolds stress profile,

$$\tau_0 = -\rho_f \left[(1 - \bar{c}_{(y)}) \overline{u_f v_f}_{(y)} + \frac{\rho_p}{\rho_f} \bar{c}_{(y)} \overline{u_p v_p}_{(y)} \right] \Big/ (1 - y/h) \tag{3}$$

where $\bar{c}_{(y)}$ is the mean volumetric concentration at distance y from the wall (u and v are used for the fluctuating velocity components, and u' and v' for the r.m.s. values). In (3), the viscous stress term was not considered because the friction velocity was determined by an extrapolation down to the wall of the total stress measured for $y/h > 0.1$; in this region, the viscous stress is negligible in comparison to the Reynolds stress.

The results of these evaluations are presented in table 3. As far as the clear water is concerned, the difference between the two estimates of shear velocity is less than 3%, in agreement with Nezu & Nakagawa (1993). On the other hand, for the experiments with particles (sediment-laden flow), the difference is much higher (up to 15%). This difference, especially for high particle concentrations, could depend on extra terms which should be included in (3); they take into account the mutual interactions between solid and fluid phases and other contributions (Ishii 1975). Therefore, in sediment-laden flows the measured Reynolds stress profile does not necessarily follow the classical linear trend along the flow depth and the first evaluation was preferred over the second.

3. Single-phase flow: comparison with existing results

To assess the reliability of the present measurements, a comparison with results given in the literature for the near-wall region of a single-phase flow is presented. The

https://doi.org/10.1017/S0022112004008304 Published online by Cambridge University Press

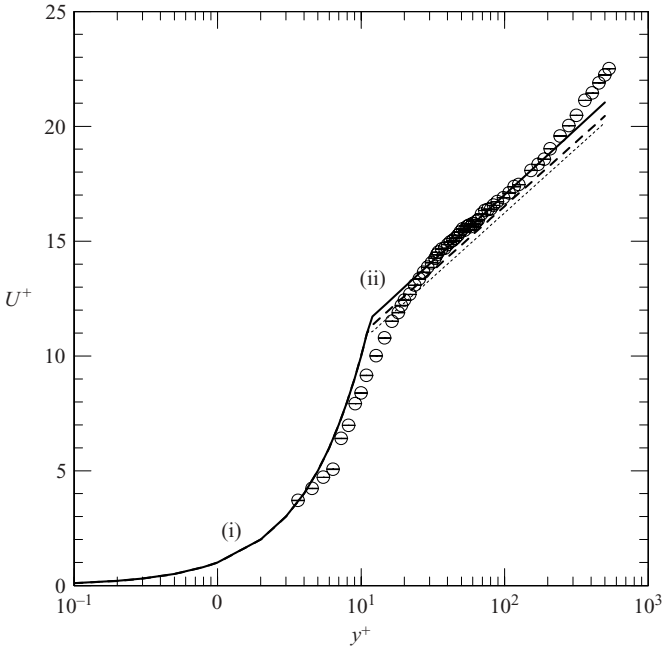


FIGURE 4. Mean velocity profile for clear water: ○, experimental data (errors are within the symbol size); (i) ——, $U^+ = y^+$; (ii) ——, Nikuradse log-law ($k = 0.4$, $B = 5.5$); - - - - -, Nezu & Rodi log-law ($k = 0.41$, $B = 5.29$); ..... Coles log-law ($k = 0.41$, $B = 5$).

clear-water data are acquired with exactly the same set-up as used for the two-phase flow but without solid particles in the flow.

In figure 4, the experimental values of the mean streamwise velocity profile U^+ are reported and compared with the 'classical' logarithmic and linear laws of the wall:

$$U^+ = U/u^* = \frac{1}{k}\ln(y^+) + B, \quad U^+ = y^+, \tag{4}$$

where usually $k = 0.41$ and B ranges between 5 and 5.5 (Nezu & Nakagawa 1993). In particular, the experimental values are compared with (4), where the values of k and B proposed by Nikuradse (see e.g. Nezu & Nakagawa 1993), Coles (1968) and Nezu & Rodi (1986) are assumed.

The overall behaviour derived from the present data agrees with these results; more particularly, for the log region ($30 < y^+ < 200$), the von Kármán constant is $k \approx 0.4$ and the coefficient is $B \approx 5.5$ in agreement with the results from previous authors. In the outer part ($y^+ > 200$), the data deviate from the logarithmic law due to the effect of the free surface (placed at about $y^+ \approx 850$), while at the lower end, the minimum distance from the wall is about 3 wall units.

In figure 5, the profiles of r.m.s. streamwise and vertical velocities are given together with the experimental results obtained by Laufer (1950), Wei & Willmarth (1989) and Karlsson & Johansson (1986) at nearly the same Reynolds numbers. The different results agree satisfactorily over the entire range. However, there is some disagreement between the different data sets for $y^+ > 100$ which could reflect the different boundary conditions and the strong dependence of the external flow on the Reynolds number. On the other hand, for $y^+ < 20$, especially for the streamwise velocity, there is no complete data overlapping. First, it should be noted that even among the other data

https://doi.org/10.1017/S0022112004008304 Published online by Cambridge University Press

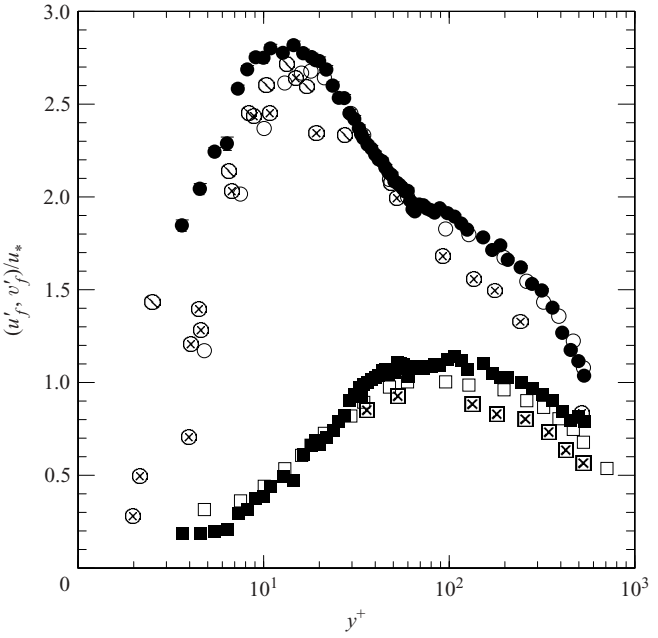


FIGURE 5. R.m.s. profiles of the streamwise (u'_f) and vertical (v'_f) velocity components for clear water (errors are indicated by vertical bars, mostly within symbol size): ●, u'_f; ■, v'_f; ○, u'_f Wei & Willmart (1989) $Re=14\,914$; □, v'_f Wei & Willmart (1989) $Re=14\,914$; ⊘, u'_f Karlsson & Johansson (1986) $Re=17\,300$; ⊗, u'_f Laufer (1950) $Re=12\,300$; ⊠, v'_f Laufer (1950) $Re=12\,300$.

sets the agreement is not particularly good, for example in respect to the location and amplitude of the maximum. Moreover, considering measurement errors (indicated by vertical bars), the present measurements agree satisfactorily with those of Wei & Willmarth (1989) and of Karlsson & Johansson (1986).

The comparison for the Reynolds stress cross-moment is presented in figure 6. This quantity, compared with the previous mean and r.m.s. velocities, is much more sensitive to measurement errors. The present measurements are compared with other authors as for the r.m.s. velocities, and the differences are quite small. The region where the absolute value of the Reynolds stress is maximum (note that the vertical scale has been multiplied by -1) is $40 < y^+ < 80$ in agreement with the results by Wei & Willmarth (1989) and slightly smaller than in Karlsson & Johansson (1986).

From the comparisons of figures 4 to 6, it is concluded that the experimental set-up used for the present measurements is able to reproduce the well-known results for a near-wall single-phase flow. In the next section, interest will focus on the modification of the velocity moment profiles when solid particles are added to the flow.

4. Results for two-phase flow

As in the Introduction, the results will be presented separately for mean velocity, mean velocity differences, r.m.s. fluctuations and Reynolds stress.

4.1. *Mean velocity profile*

The mean velocity profiles for the 100 and 200 μm particles are given in figure 7 using the same variables as figure 4. The contributions of the solid and fluid phases (when

https://doi.org/10.1017/S0022112004008304 Published online by Cambridge University Press

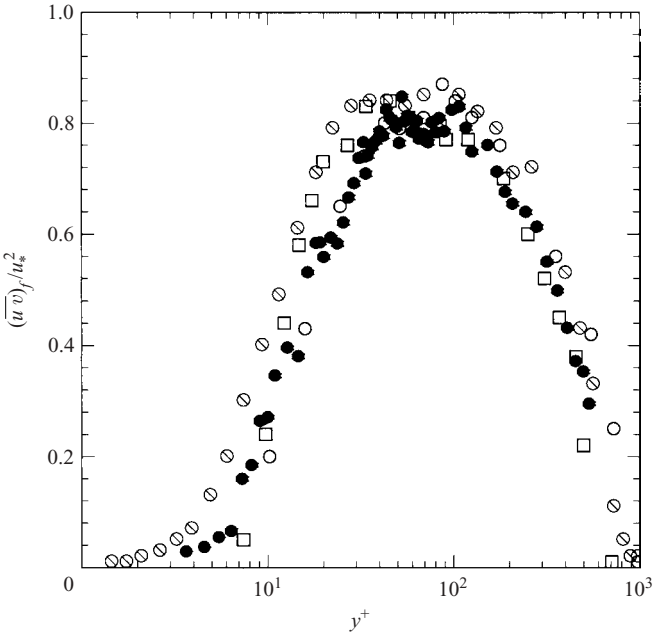


FIGURE 6. Reynolds stress profile for clear water: ●, experimental data (errors are indicated by vertical bars and are within the symbol size); □, Wei & Willmart (1989) $Re = 14\,914$; ○, Wei & Willmart (1989) $Re = 22\,776$; ⊘, Karlsson & Johansson (1986) $Re = 17\,300$.

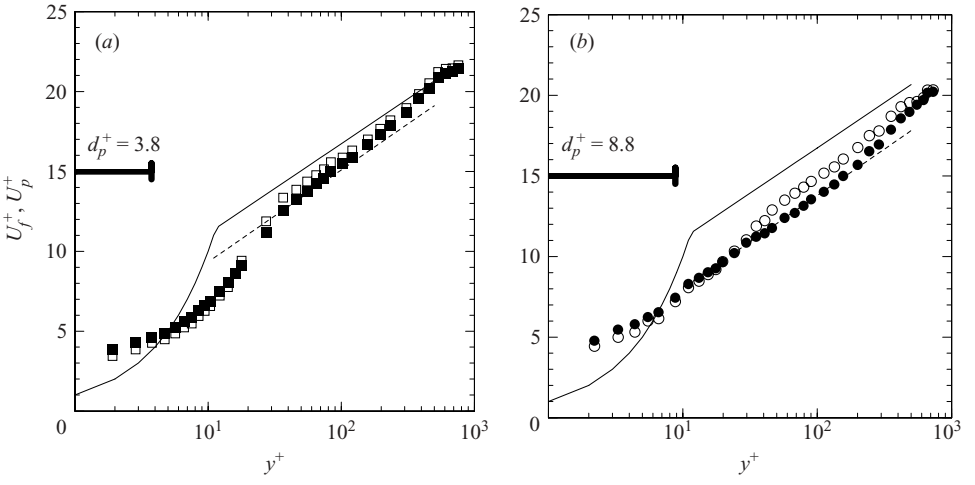


FIGURE 7. Mean velocity profiles for (*a*) the 100 μm and (*b*) the 200 μm particles; solid symbols are for the solid phase and open symbols for the fluid phase: ——, linear law and Nikuradse log-law ($k = 0.4$, $B = 5.5$); - - - - -, White's log-law ($k = 0.4$, $B = 5$, $d^+ = 3.8$ and $d^+ = 8.8$ for the 100 μm and 200 μm particles respectively).

particles are present) are separated and compared with the laws of the wall and the law of White (1974):

$$U^+ = \frac{1}{k}\ln(y^+) + 5.5 - \frac{1}{k}\ln(1 + 0.3d^+) \tag{5}$$

https://doi.org/10.1017/S0022112004008304 Published online by Cambridge University Press

valid for clear water with wall roughness equal to the dimensionless particle size d^+ (as given in table 2, for the present particles this is approximately equal to 4 and 9 respectively for the 100 and 200 μm particles). The figure shows that the velocity profiles of fluid and solid phases decrease, compared with the clear-water case, similarly to the observations of Coleman (1986), Valiani (1991), Muste & Patel (1997) and Best *et al.* (1997).

For the fluid phase, the decrease in the logarithmic region is almost independent of the distance from the wall and the von Kármán constant k remains equal to about 0.4. The effect of particles is also to erode the extent of the logarithmic law, from the bottom (i.e. the buffer zone) and from the top (i.e. the wake region). Moreover, the amount of the decrease is smaller than the prediction (5), i.e. by assuming a wall roughness equivalent to the particle diameter. This indicates that the effective wall roughness should be less than d^+ (about $d^+/2$), in contrast with the results of Muste & Patel (1997) and Best *et al.* (1997) who indicated an equivalent wall roughness equal to $2d^+$. However, this is not surprising, since in the present conditions the bed is not fully covered by particles.

In accordance with (5), the logarithmic profile is expected to lower as the particle size (d^+) increases; using such a relation, the velocity difference between the two sediment-laden experiments (100 and 200 μm particles), ΔU^+, is computed as $\Delta U^+ \approx -1.4$. This value is almost identical to the one derived from the observed experimental difference within the range $30 < y^+ < 200$ (figure 7).

For $y^+ < 30$, the velocity profile for the small particles (100 μm) moves from the logarithmic to a linear behaviour, whereas for the 200 μm particles no linear law is observed. The streamwise velocity profile in the inner region ($y^+ < 5$) indicates that the particle-laden flow exhibits a velocity close to the wall which is significantly larger than in clear-water conditions (almost twice as much). This behaviour suggests that particles slide and roll on the wall when moving downstream, driving the surrounding fluid; in this case, an apparent slip boundary condition is more appropriate than a non-slip condition for an effective description of the kinematic boundary condition at this distance from the wall ($y^+ \approx 2$). The velocity of the solid phase is higher than that of the fluid close to the wall ($y^+ < 20$) and lower in the outer part of the flow ($y^+ > 20$); these results agree with previous measurements (Rashidi *et al.* 1990; Niño & Garcia 1996; Best *et al.* 1997).

These results on the mean flow seem to indicate that an enhanced wall roughness due to particles could account for the observed behaviours, but the amount of the observed differences is not fully explained. From this point of view, the differences between the fluid and solid phases are of great significance and must be considered in detail.

4.2. *Differences between particle and fluid mean velocities*

A better insight into the kinematics of heavy particles is achieved by considering figure 8, where the streamwise velocity difference between fluid and solid is plotted for the two particle sizes. In the figure, the different values attained by the Stokes number are also indicated; to evaluate the Stokes number, the characteristic time of energy-containing eddies is roughly estimated by the relation $t_e \approx k y^+ \nu / u^{*2}$ (Tennekes & Lumley 1972). In a layer close to the wall ($y^+ < 20$), with an extent almost independent of the particle size, the particles are faster than the fluid (the difference between the two velocities is up to $0.4u^*$). This difference (which is slightly lower for the largest size particles) is approximately constant when approaching the wall. Across the region $20 < y^+ < 50$ (the amplitude of this interval seems to depend on the Stokes number, i.e.

https://doi.org/10.1017/S0022112004008304 Published online by Cambridge University Press

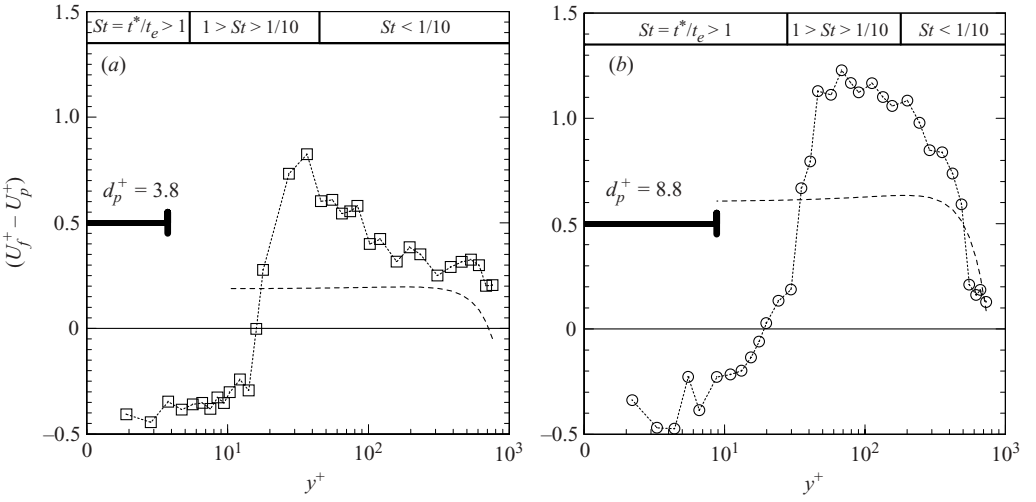


FIGURE 8. Difference between mean velocity of the fluid and solid phases for (*a*) the 100 μm (*b*) the and 200 μm particles. The regions with different values of the Stokes number are indicated. The dashed lines represent predictions by the model of Greimann *et al.* (1999).

on the particle size), there is an abrupt change in the sign of the fluid–particle velocity difference and the fluid becomes faster than the particles (the velocity difference is between $0.8u^*$ and $1.2u^*$). Here, the maximum velocity differences are achieved; the 100 μm particles show a velocity lag which is about 1.5 times lower than the larger particles. This region is the one where wall-burst phenomena are stronger. Moving further from the wall, in the region where the Stokes number is smaller than 1/10, the fluid–particle velocity difference decreases to zero.

The present results are somewhat complementary to those by Muste & Patel (1997); the observed velocity difference scales with the particle size (while referring to an almost constant depth-average volumetric concentration), whereas Muste & Patel (1997) consider constant particle diameter and derive a lag which increases with the particle concentration. Moreover, they looked at the outer part of the wall region ($y^+ > 200$) and did not notice the inversion of the velocity lag which is observed in the present measurements. The analytical prediction derived for very small Stokes number by Greimann *et al.* (1999) is also included in the figure; it describes reasonably well the measured velocity lag for both particle sizes in the outer region where $St < 1/20$. On the other hand, their prediction of a constant velocity difference in the inner layer is not fulfilled.

This behaviour could be explained as follows; far from the wall ($y^+ > 200$), the solid particles follow quite accurately and immediately fluctuations of the fluid velocity field, the time scale for particle modifications (particle relaxation time) being much smaller than the characteristic eddy time scale ($St \ll 1$). When moving closer to the wall ($20 < y^+ < 100$), where the velocity fluctuations are larger than far from the wall (see the next section), the particles are not longer able to respond promptly to the turbulent fluctuations, thus exhibiting an increasing deviation from the fluid velocity ($St \leqslant 1$). Such a velocity lag can be explained if the particle motion is associated with the dynamics of the wall vortical structures. As reported in the model by Adrian *et al.* (2000), flow ejections are related to the velocity field induced by a primary hairpin and represent the dominating part of the near-wall dynamics at these distances from

https://doi.org/10.1017/S0022112004008304 Published online by Cambridge University Press

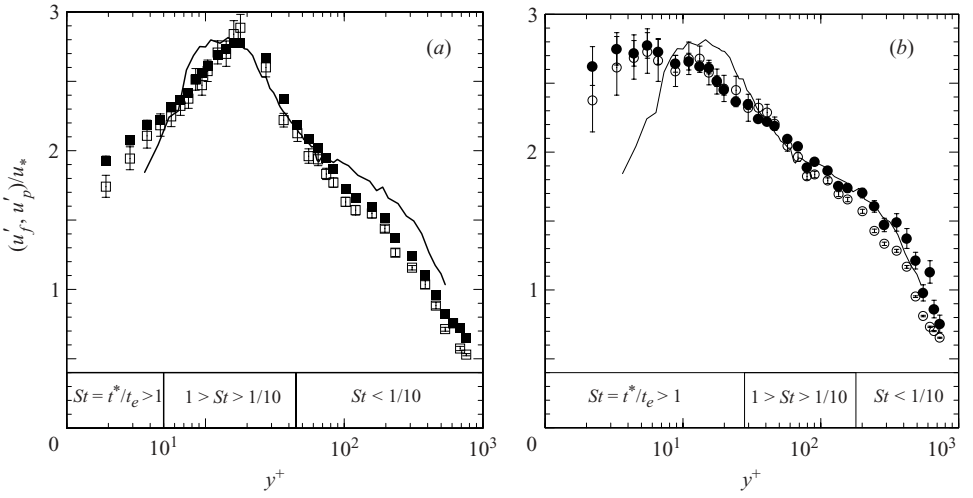


FIGURE 9. R.m.s. profiles of the streamwise velocity component for (*a*) the 100 μm and (*b*) the 200 μm particles, compared with clear-water measurements; solid symbols are for the solid phase and open symbols for the fluid phase (errors are indicated by vertical bars); ——, clear-water measurements.

the wall (Lu & Willmarth 1973). In this region, the particles are convected and lifted up by ejections of low-momentum fluid from the wall region; due to their inertia ($St \leqslant 1$), they are affected by such a low momentum, thus exhibiting a velocity lag in comparison to the surrounding fluid. In the very near-wall region ($y^+ < 10$), injections of high-momentum fluid dominate the wall dynamics; high-momentum particles are carried along the wall by such events. These particles respond very slowly to the local velocity field and, due to their inertia, they retain their velocity which is higher than that of the surrounding fluid ($St > 1$). This leads to the non-zero longitudinal mean velocity at the wall and to the slip boundary condition which was described in the previous section. This mechanism is similar to that provided by Kulick *et al.* (1994), i.e. a transfer of momentum due to the solid particles moving towards the wall from the faster upper layer. The momentum exchange between solid and fluid phase will be investigated in the next two sections.

4.3. *Fluctuating velocity components*

The dimensionless r.m.s. velocity fluctuations along the streamwise and vertical directions are given in figures 9 and 10 together with the corresponding clear-water profiles.

For the streamwise component (figure 9), from the outer region down to $y^+ \approx 30$, the fluctuations of both fluid and solid phases in particle-laden conditions are similar to those in clear water (a very slight damping is noticed in this region for both the size classes in comparison to the clear-water profile). Closer to the wall, these fluctuations are first damped ($7 < y^+ < 20$) and then enhanced ($y^+ < 7$) in comparison to the clear-water profile by amounts which increase with the particle size. Accordingly to Owen (1969), the region where substantial modifications of the streamwise fluctuation profile are observed roughly corresponds to $t^* > t_e$ or $St > 1$ (the intervals for the different values of the ratio $St = t^*/t_e$ are also reported in the figure). Moreover, in the logarithmic region the ratio of particle diameter to flow integral length scale is much smaller than 1 thus indicating that the predictions by Gore & Crowe (1989)

https://doi.org/10.1017/S0022112004008304 Published online by Cambridge University Press

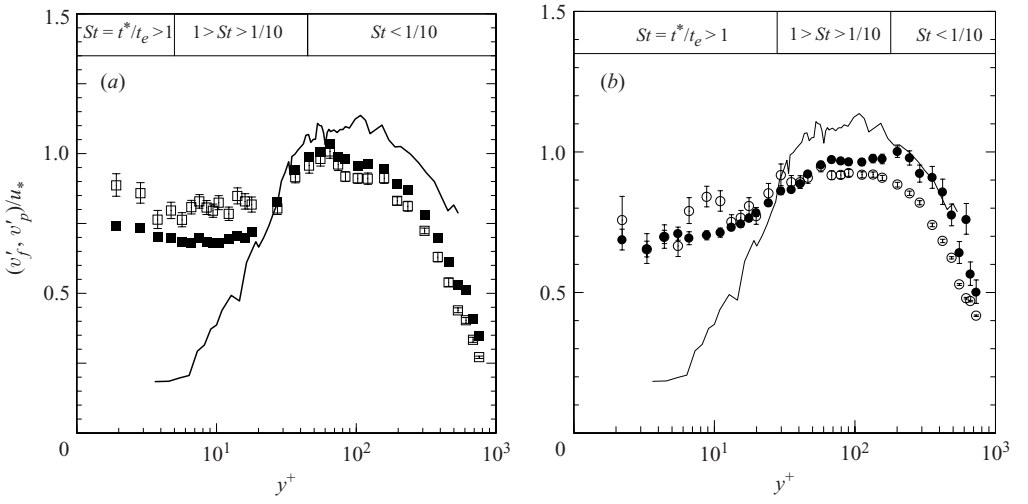


FIGURE 10. R.m.s. profiles of the vertical velocity component for (*a*) the 100 μm and (*b*) the 200 μm particles, compared with clear-water measurements; solid symbols are for the solid phase and open symbols for the fluid phase (errors are indicated by vertical bars); ——, clear-water measurements.

of a damping of fluctuations are verified. It is important to notice that, in the present particle-laden conditions, the streamwise r.m.s. velocity of the solid phase is consistently larger than that of the fluid, all along the vertical profile. Comparing the behaviours of the 100 and 200 μm particles, they are quite similar except for $y^+ < 7$ (where a larger difference of the latter in respect to the clear-water profile is observed) and in the region $20 < y^+ < 50$ (where the r.m.s. fluctuations of the 100 μm particles are larger (or equal) than the clear-water case, whereas those of the 200 μm are smaller).

For the vertical fluctuations in particle-laden conditions (figure 10), down to $y^+ \approx 30$ the damping in comparison to the clear-water profile is stronger than for the streamwise fluctuations (more than 20%) for both size classes. In contrast to the horizontal fluctuations, substantial modifications of the vertical fluctuation profile are already observed for $0.1 < St < 1$. This is not what can be expected for rough walls, where velocity fluctuations in the outer region are enhanced rather than damped (Nezu & Nakagawa 1993; Krogstad & Antonia 1999); therefore, in the outer region the effect of the solid phase cannot be represented merely by an increased wall roughness. For $y^+ < 30$, a strong enhancement of vertical velocity fluctuations (almost independent of the particle size) is noticed. Moreover, in particle-laden conditions, while in the outer region the fluctuations of the solid phase are larger than those produced by the fluid, in the region $y^+ < 30$ they are smaller. The comparison between the r.m.s. vertical fluctuations of the 100 and 200 μm particles indicates that (similarly to the longitudinal r.m.s.) they are quite similar except for the region $20 < y^+ < 50$.

To explain these observations, it is necessary to follow the considerations outlined in the previous section, i.e. that the solid particles are mainly driven by the fluid wall dynamics (mean field, as depicted in figures 7 and 8). As a consequence, particles carry momentum and momentum fluctuations from the regions they are leaving. In this sense, the behaviour of the particles at a given distance from the wall is influenced by that of the fluid at another distance if there is a dynamic connection between the

https://doi.org/10.1017/S0022112004008304 Published online by Cambridge University Press

two; as pointed out in the dynamical model by Adrian *et al.* (2000), this connection is particularly effective for $y^+ < 200$.

Therefore, if this point of view is admitted, in order to explain the behaviour of the turbulence intensity (fluctuating field) in the buffer and in the outer region ($y^+ > 20$), the behaviour in the very near-wall region cannot be neglected. Providing that the intense fluid ejections from the inner wall region lift up the solid phase, the differences in time scales between the fluid and the particles ($St \leqslant 1$) indicate that the latter retain the low-momentum and the high-velocity fluctuations experienced by the fluid during the bursting events. This circumstance could explain why in the outer region the particle r.m.s. fluctuations are systematically larger than those of the fluid, along both longitudinal and vertical directions. Nonetheless, fluctuations are still smaller than in clear water; this is due to ejected lumps of fluid which have to use part of their vertical momentum to overcome the gravity force and to lift up the solid particles. The longitudinal particle–fluid velocity differences suggest that, at the same time, a momentum exchange between the two phases in the streamwise direction also occurs. The observation that in particle–laden conditions both the streamwise but especially the vertical fluid fluctuations are damped in comparison to the clear water (in the outer region), suggests that this momentum exchange is more effective along the vertical. Owing to this momentum exchange, part of the turbulent kinetic energy produced during the bursting events is transferred to the particles and it is no longer at disposal of the turbulent diffusion process which takes place in the outer layer.

Concerning the region $y^+ < 15$, the high velocity fluctuations at $y^+ \approx 20$ are carried by the solid particles towards the wall through fluid sweeps. Due to their inertia ($St > 1$), the particles respond rather slowly to the local field and therefore, during their hitting and rebounding, they induce large fluctuations in the fluid phase by retaining memory of the higher momentum they had from the outer layer and by giving rise to local deviations of the fluid velocity field (particle presence effect). Nevertheless in this region, regarding particle and fluid r.m.s. fluctuations in particle-laden conditions, there are differences between longitudinal and vertical components; streamwise particle velocity fluctuations are larger than those of the fluid, thus confirming that the particle inertia increases the local longitudinal momentum fluctuations (as for $y^+ > 20$ and similarly to the velocity defect described in the previous section). On the other hand, the vertical particle velocity fluctuations are smaller than those of the fluid; this effect can be related to the limited extent of the particle vertical motions in the near-wall region due to the gravity force (which limits upwards motions) and to the presence of the wall (which limits downwards motions) (Tsuji & Morikawa 1982; Tsuji *et al.* 1984; Niño & Garcia 1996).

Regarding the comparison between the two size classes (100 and 200 μm), it is important to remark that the particles with the highest inertia (i.e. the 200 μm particles as confirmed by the largest value of the ratio w_s/u^* given in table 2) must retain much more of their former momentum levels when moving under the wall dynamics phenomena. This could explain why the r.m.s. fluctuations close to the wall increase with the particle size especially for the longitudinal fluctuations, but rather less for the vertical which are bounded by the wall and by the gravity force as described above.

From the spectral point of view, due to the well-known low-pass filter effect exhibited by the particle spectrum in comparison to that of the fluid and to the measured particle velocity fluctuations (Kulick *et al.* 1994), in particle-laden conditions there could be an increment of the low-frequency spectral content. If the previous explanations were correct, this increment would be related to contributions from the

https://doi.org/10.1017/S0022112004008304 Published online by Cambridge University Press

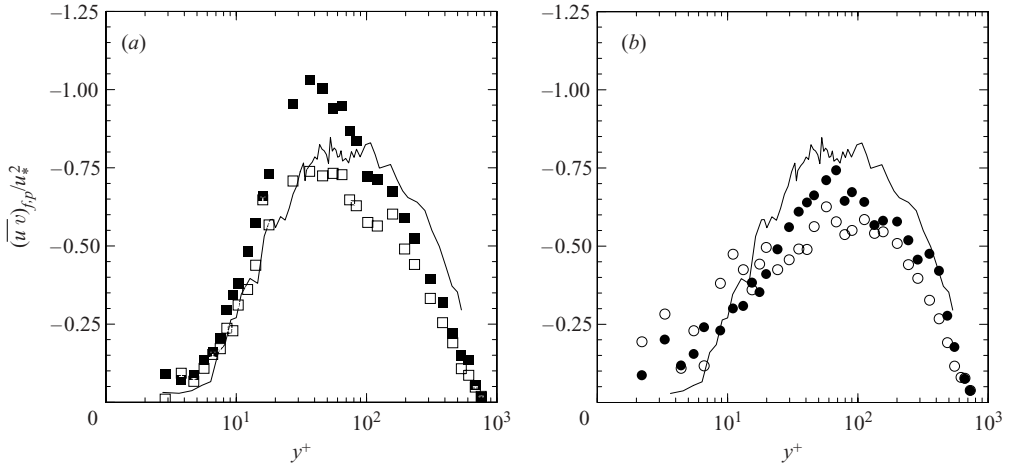


FIGURE 11. Reynolds stress profiles for (*a*) the 100 μm and (*b*) the 200 μm particles, compared with clear-water measurements; solid symbols are for the solid phase and open symbols for the fluid phase; ——, clear-water measurements.

regions where the momentum fluctuations are the largest ($y^+ \approx 10$–20) and it should be effective for both $y^+ > 20$ and $y^+ < 20$ (except for the mentioned limitation on the vertical fluctuations). Thus, in comparison to the clear-water conditions, the energy would be re-distributed, to a greater or lesser extent, from the region of maximum energy production.

The previous explanations of the observed results in terms of fluid wall dynamics call for an investigation of wall events using measurements of the Reynolds stress.

4.4. *Reynolds stress and near-wall turbulence*

Sediment-laden Reynolds stress profiles for the 100 and 200 μm particles in comparison to that of the clear-water profiles are shown in figure 11. In the region $y^+ < 10$, for both size classes, the Reynolds stresses of the fluid (with particles) and of the solid phases are enhanced in comparison with the clear-water data; this effect is similar to that observed in the r.m.s. profiles, the amount of the differences being lower. In the region $y^+ > 10$, the Reynolds stress profile of the fluid (with particles) is reduced in comparison to the clear-water profile by an amount which seems to depend on the particle size.

Regarding the differences between the clear-water and the solid-phase profiles, in the region $10 < y^+ < 200$, the Reynolds stress profile of the solid phase is higher than the clear water for the 100 μm particles, while is lower for the 200 μm particles; on the other hand, for larger distances from the wall, the Reynolds stress profiles of both sizes are lower. The comparison between the Reynolds stress profiles of the fluid and solid phase in sediment-laden flow reveals that in the region $y^+ > 10$ the former is smaller than the latter, whereas for $y^+ < 10$ the difference weakens and almost vanishes for the measurements close to the wall.

These observations fall well within the picture outlined previously when considering r.m.s. profiles; if the wall dynamics events are responsible for the particle vertical motion towards and from the wall and if the particle inertia accounts for storage and recovery, then in comparison to the clear-water conditions, close to the wall there should be an increment of the Reynolds stress and far from the wall there should be a reduction (as observed). Moreover, due to inertia, the differences between the two size

https://doi.org/10.1017/S0022112004008304 Published online by Cambridge University Press

classes must depend on the particle size; for the small particles (100 μm) the deviation from the clear-water conditions must be less noticeable than for the larger (200 μm). The results presented in figure 11 show that this is always true except for the region where the wall dynamics lift-up phenomena are dominating (i.e. $20 < y^+ < 100$). A possible explanation could be the different lift-up properties of the particles; in this region, due to the smaller ratio between Stokes and friction velocities ($w_s/u^* = 0.3$ for 100 μm and $w_s/u^* = 0.9$ for 200 μm as reported in table 2), particles are lifted up especially by the strong ejections. The small particles react more promptly than the large ones to the abrupt accelerations during ejections, thus exhibiting a higher Reynolds stress profile (even larger than in the clear-water case due to the fact that weak ejections do not lift particles). For the reasons outlined above (wall dynamics and particle inertia), in sediment-laden flow, the particles retain larger Reynolds stress values than the fluid.

In order to gain a deeper insight into the mechanisms specifically involved in particle motion close to the wall, a quadrant analysis of the Reynolds stress is performed (Lu & Willmarth 1973). At each distance from the wall, the average contribution to the Reynolds stress of the ith quadrant on the (u, v)-plane can be evaluated as

$$\overline{uv}_{i(H)} = \lim_{T\to\infty} \frac{1}{T} \int_0^T uv_{i(t)} S_{i(t,H)}\, \mathrm{d}t, \quad i = (1, 2, 3, 4), \tag{6}$$

where $uv_{i(t)}$ is the contribution of the Reynolds stress to the ith quadrant, T is the acquisition time interval and the function S is defined as $S_{i(t,H)} = 1$ if $|uv|_i > Hu'v'$ and $S_{i(t,H)} = 0$ otherwise (where $|uv|_i$ indicates the absolute value). The sum of contributions from all quadrants must be exactly equal to the total Reynolds stress. The threshold level H (defined in terms of the local r.m.s. velocity fluctuations u' and v'), which is a crucial parameter for such an analysis, has been changed between 0 and 1. The value $H = 1$ is usually accepted (in clear water) in order to distinguish ejections and sweeps events from non-coherent ejection-like and sweep-like turbulence; equivalent values for the threshold level are not yet unambiguously defined for sediment-laden flows due to the fact that the r.m.s. values (u' and v') are strongly changed in such conditions (as outlined in § 4.3). For this reason, considering moreover that the conclusions derived from the choice $H = 1$ are indistinguishable from those with $H = 0$, the latter unambiguous value has been used.

Another average can be evaluated by computing the intensity of the ith quadrant, i.e. by weighting the Reynolds stress with the time spent within the quadrant itself (T_i):

$$\langle uv \rangle_{i(H)} = \lim_{T\to\infty} \frac{1}{T_i} \int_0^T uv_{i(t)} S_{i(t,H)}\, \mathrm{d}t = \frac{T}{T_i} \overline{uv}_{i(H)}, \quad i = (1, 2, 3, 4), \tag{7}$$

where the sum of all contributions, $\langle uv \rangle$, is now different from the total Reynolds stress, due to the time-weighting. The aim of the quadrant analysis is to achieve a deeper insight into the possible reasons for damping effects acting on the turbulence structure and on the mechanisms of entrainment due to the solid particles; from this point of view, the intensity of Reynolds stress is considered a better indicator than the average contribution.

In figure 12, the quadrant profiles (obtained using relation (7)) are shown for the fluid phase of the 100 and 200 μm particles and compared to the result in clear-water conditions; the results obtained in clear-water are in agreement with those of Lu & Willmarth (1973) for a smooth bed. The quadrant profiles for clear-water and sediment-laden conditions have a similar behaviour; however, all quadrant intensities

https://doi.org/10.1017/S0022112004008304 Published online by Cambridge University Press

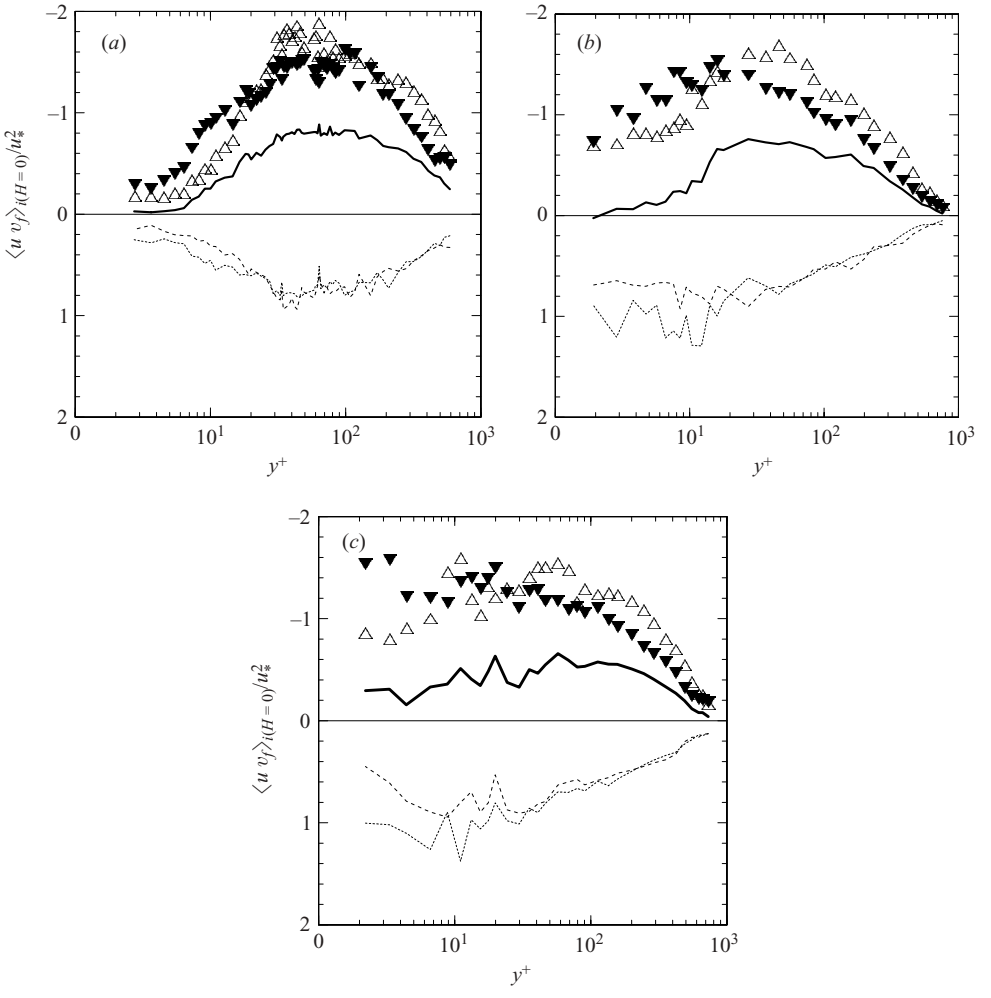


FIGURE 12. Profiles of intensity of Reynolds stress from each quadrant for (*a*) clear water, and the fluid phase of (*b*) the 100 μm and (*c*) the 200 μm particles: ....., quadrant I; △, quadrant II; - - - - -, quadrant III; ▼, quadrant IV; ——, total Reynolds stress.

in the sediment-laden profiles are enhanced for $y^+ < 20$ (similarly to r.m.s. and Reynolds stress profiles). In particular, close to the wall, the second ($u < 0$, $v > 0$) and fourth ($u > 0$, $v < 0$) quadrant events have intensities more than two times larger than in clear-water conditions. As is well-known, a second quadrant event corresponds to an ejection, and a fourth quadrant one to a sweep (Lu & Willmarth 1973). The crossover between the second and fourth quadrants and between the first and third quadrants at $y^+ \approx 20$ is almost unaffected by the particles. In the region $20 < y^+ < 200$, there is an overall damping of the quadrant intensities, which is especially appreciable for the second quadrant (at $y^+ \approx 40$ about 30%). The effects described are observed to increase with the particle size.

As conjectured in the previous sections, the wall dynamics phenomena have a complex interaction with the solid particles; in particular, the flow ejections (second quadrant) are responsible for particle lift-up and are supposed to pass a significant part of their momentum to the particles. Thus, as observed, ejections are expected

https://doi.org/10.1017/S0022112004008304 Published online by Cambridge University Press

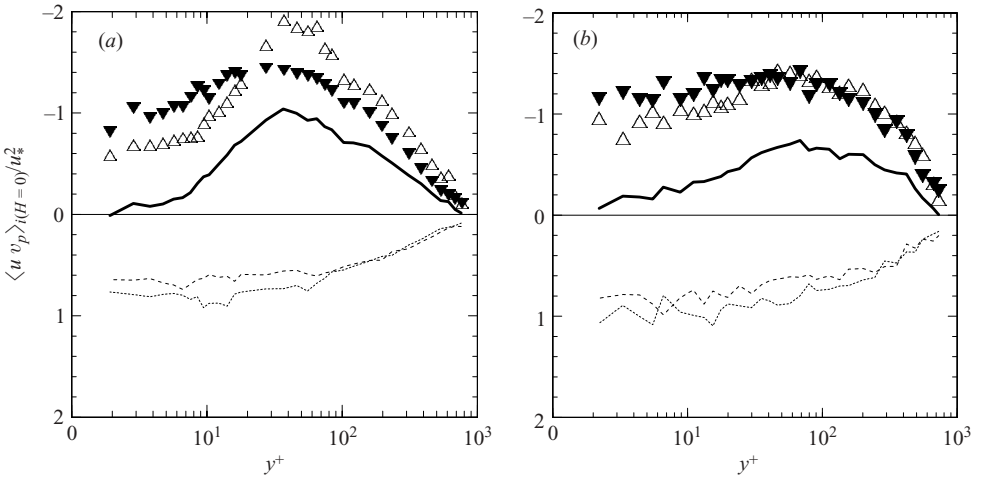


FIGURE 13. Profiles of intensity of Reynolds stress from each quadrant for the solid phase of (*a*) the 100 μm and (*b*) the 200 μm particles: ....., quadrant I; △, quadrant II; - - - - -, quadrant III; ▼, quadrant IV; ——, total Reynolds stress.

to be damped in sediment-laden conditions, whereas this phenomenon must be less effective for sweeps (fourth quadrant).

In figure 13, the quadrant analysis is given for the solid phase for both particle size classes. The profiles of the solid phase are quite close to those of the fluid phase presented in figure 12 for all quadrants (thus confirming that the dynamics of the fluid and of particles are coupled), except for the second quadrant of the 100 μm particles. The behaviour of the second quadrant data deserves particular attention: especially in the region $20 < y+ < 200$, the second quadrant intensity of the 100 μm particles is significantly larger than that of the fluid phase (with particles) and this could be an indication that the solid particles are lifted by strong ejections. On the other hand, for the 200 μm particles, the relevance of the second quadrant events is not noticed. Such a different behaviour is probably due to the different inertia and weight of the particles: the greater the particles, the stronger the ejection which is required to lift them. Meanwhile, the particle response to the sudden accelerations due to the effective ejections becomes more and more misleading as their inertia increases.

The relative influence of each quadrant is determined by subdividing the wall layer into the inner ($y^+ < 10$), buffer ($10 < y^+ < 30$), logarithmic ($30 < y^+ < 100$) and outer ($y^+ > 100$) regions. In each one, the relative averaged intensity of each quadrant is evaluated by considering point by point the absolute values for that quadrant divided by the sum of the four corresponding absolute values, averaged over the measurement points within each region; the result of this operation is shown in figure 14 for the three layers closest to the wall. For the outer layer the results are similar to those of the logarithmic region. For the clear-water flow (particle size equal to 0), it is observed that close to the wall ($y^+ < 10$) the averaged intensity from all quadrants is similar except for the fourth quadrant which is the largest, whereas for $y^+ > 10$ the second and fourth quadrant averaged intensities dominate. In particular, in the region $10 < y^+ < 30$, the fourth quadrant events (sweeps) have the largest significance, whereas for $y^+ > 30$ this happens for the second quadrant (ejections).

The previous observations are also valid for particle-laden flows; however, the relative averaged intensity of each quadrant changes substantially as a function of the

https://doi.org/10.1017/S0022112004008304 Published online by Cambridge University Press

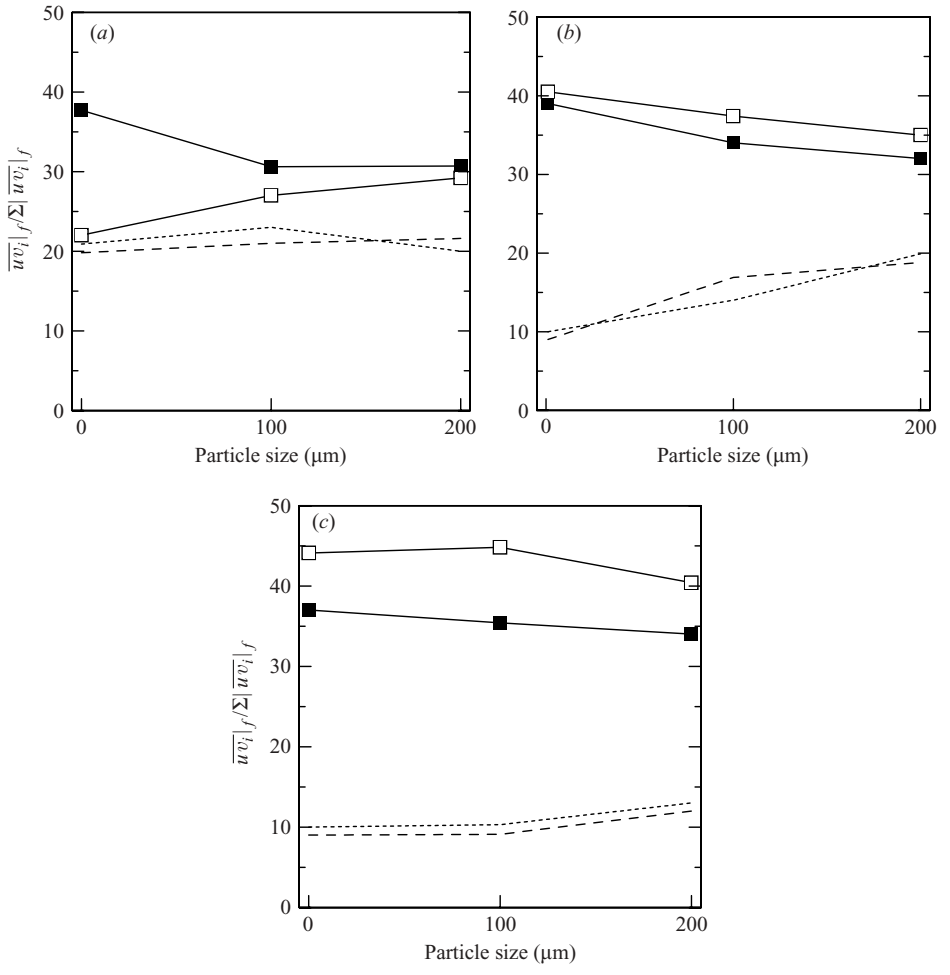


FIGURE 14. Contribution (absolute values) of each quadrant to the Reynolds stress as a function of the particle size for the fluid phase at (*a*) $y^+ < 10$, (*b*) $10 < y^+ < 30$ and (*c*) $30 < y^+ < 100$: ....., quadrant I; □, quadrant II; – – –, quadrant III; ■, quadrant IV.

particle size. In the region $y^+ < 10$, the ejection (second quadrant) averaged intensity is enhanced by the presence of the particles and, consequently, the averaged intensity of the sweeps (fourth quadrant) is suppressed (they have the same relevance for the 200 μm particles). Nevertheless, in this near-wall region, the possibility of a relevant contribution of large ejections to the particle dynamics should be rejected. Among the other possible mechanisms to explain this effect, the particle rebounding at the wall should be considered as reported by Rizk & Elgobashi (1985) and Kulick *et al.* (1994). As a consequence of a sweep event, the falling particles rebound at the wall, thus producing a sort of spurious ejection-like event even at this near-wall location. However, the present data do not allow one to clarify if this mechanism is effectively active. On the other hand, in the region $10 < y^+ < 30$ (and to a lesser extent in the region $30 < y^+ < 100$), the whole 'coherent' averaged intensity of the fourth but especially of the second quadrant is reduced in comparison to the 'incoherent' part; it decreases from 78% to 67% respectively for the clear water and the 200 μm particles (accordingly the 'non-coherent' averaged intensity increases from 22% to 33%). This

https://doi.org/10.1017/S0022112004008304 Published online by Cambridge University Press

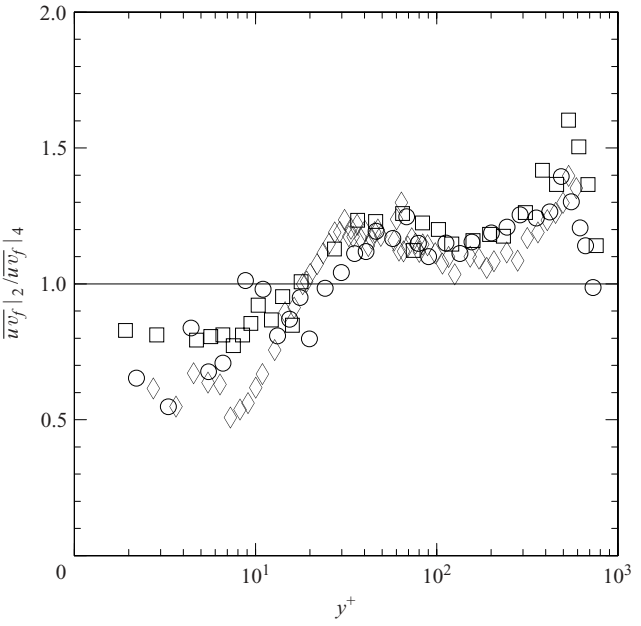


FIGURE 15. Profiles of the ratio between average contribution to Reynolds stress from second and fourth quadrants for clear water, 100 μm and 200 μm particles: ◇, clear water; ○, 100 μm fluid phase; □, 200 μm fluid phase.

effect is consistent with the previously described phenomenon of a reduction in the intensity of fluctuations and Reynolds stress as a consequence of the fluid momentum loss due to particle lift-up.

The ratio between the average contribution of second and fourth events is given in figure 15 for the three cases (clear water, 100 and 200 μm particles, the last two for the fluid phase only); this is the ratio between 'coherent' event contributions. In clear-water conditions, this ratio is almost constant (in the range 1.2–1.5) within the region $50 < y^+ < 200$ and towards the wall decreases to about 0.5; these results are in substantial agreement with those provided by Lu & Willmarth (1973) and Nakagawa & Nezu (1977).

Comparing the two-phase to the clear-water flow, in the wall region ($y^+ < 10$) an increasing relevance of ejection or ejection-like events with respect to sweeps (the average ratio goes from 0.54 for clear water to 0.73 and 0.83 respectively for the 100 and 200 μm particles) is observed; this behaviour is in agreement with the previous observations on the spurious ejection-like events which alter the dynamics of the coherent structures in this region. On the other hand, in the buffer and logarithmic regions ($10 < y^+ < 30$ and $30 < y^+ < 200$), the results for clear-water and particle-laden flows are similar for both the 100 and 200 μm particles and the relative contribution is substantially unchanged; this is not surprising, due to the fact that both 'coherent' events are reduced (as reported in figure 14).

A final remark on the quadrant analysis concerns with the differences between the solid and fluid phases when particles are present. In figure 16, the previous ratio between second and fourth quadrant contribution to the Reynolds stress is plotted for the two phases (for the 100 μm particles). For $y^+ < 10$, the ratio for the solid phase is closer to 1 than for the fluid phase, thus confirming that in the near-wall region the particles actively interact with the wall turbulent structures, inducing a higher degree

https://doi.org/10.1017/S0022112004008304 Published online by Cambridge University Press

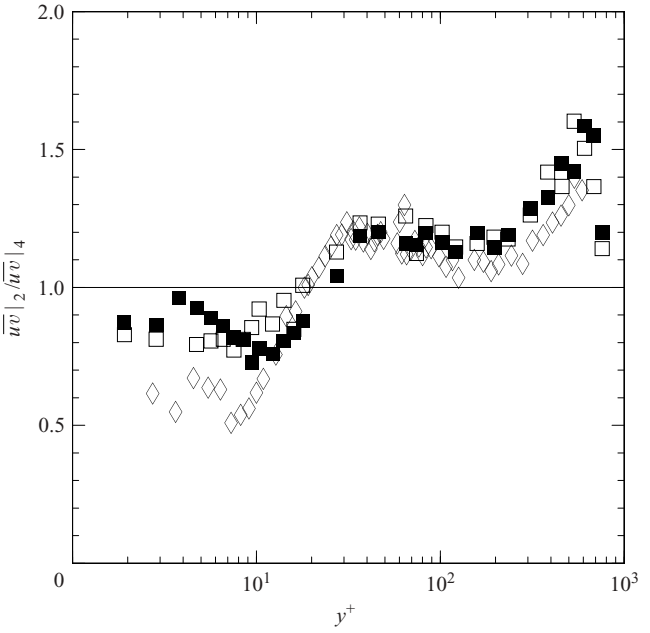


FIGURE 16. Profiles of the ratio between average contribution to Reynolds stress from second and fourth quadrants for the clear water, the fluid phase and the solid phase of the 100 μm particles: ◇, clear water; □, 100 μm fluid phase; ■, 100 μm solid phase.

of balance in the dynamics of fluid ejections and sweeps; far from the wall ($y^+ > 30$) the two phases have almost the same behaviour.

5. Concluding remarks

In this paper, experiments were performed to determine the effect of solid particles on the velocity field in near-wall turbulence. Glass spheres of diameter equal to 100 and 200 μm, with a mean volumetric concentration equal to 10^{-3}, were employed. Attention was focused on the relevance of different particle size rather than different mean concentration (which was kept constant on the average); on the other hand, the local concentration differed by more than one order of magnitude from the average when moving towards the wall and this difference could affect the particle–fluid interaction.

The experiments were performed at Froude numbers larger than 1 (supercritical regimes) to attain a plane bed configuration (without bed forms); these conditions are different from those encountered in some practical applications where the regime is subcritical. Nevertheless, it is expected that for $y^+ < 200$ the results were independent of the external flow conditions due to the fact that the wavelengths of the free-surface perturbations are much larger than the flow depth; as a consequence, the investigated flow may be considered as a boundary layer with a slight pressure gradient. The expected small effect of the Froude number on wall turbulence is also supported by the fact that in the near-wall region the present measurements in clear-water conditions (still performed at a Froude number larger than 1) are in agreement with those by other authors obtained at different Froude numbers (even smaller than 1).

The measurement technique used in the experiments was the phase Doppler anemometry (PDA) which makes it possible to distinguish between the velocity of small or large particles by simultaneously measuring their size. Thus the fluid (small particles) and solid (large particles) velocity fields can be simultaneously measured

https://doi.org/10.1017/S0022112004008304 Published online by Cambridge University Press

and compared to each other and with clear-water (without particles) conditions. The technique is point-like, non-intrusive and arises from laser Doppler anemometry (LDA); it is now well established and commonly used for measurements in sprays.

The experiments were performed at a Reynolds number equal to about 15 000 (based on the water height and on the average streamwise velocity), at which data from other authors are widely available. The minimum distance from the wall at which measurements were made was equal to about 3 wall units, i.e. well inside the viscous sublayer. Therefore, information from the present measurements either overlap some of the previous measurements, or extend to the regime of high local concentrations in the very near-wall region. The profiles of mean velocity, r.m.s. fluctuations and Reynolds stress for the clear-water condition reproduce satisfactorily previous available data.

For sediment-laden flow, the mean velocity profile in the logarithmic and outer regions exhibits a noticeable decrease, increasing as the dimensionless particle size d^+, which is in agreement with the hypothesis of considering the particles as mostly sitting on the wall and acting on the flow similarly to a rough wall (with an equivalent wall roughness almost equal to $d^+/2$). The simultaneous increase of the profile in comparison to clear water in the inner region ($y^+ < 5$) leads to a velocity gradient normal to the wall for the sediment-laden flow which is smaller than in clear water and to a non-zero velocity at a distance from the wall equal to about 2 wall units. This is a consequence of the 'sliding and rolling' particle motion at the wall which also drives the surrounding fluid; thus, in sediment-laden flows a slip kinematic boundary condition at $y^+ \approx 2$ seems to be more effective than the non-slip condition for both fluid and solid phases.

Regarding the differences between the velocity of the fluid and of the particles, it has been measured that this difference is negative (particles are faster than fluid) close to the wall ($y^+ < 20$), while it becomes positive (fluid faster than particles) further from the wall ($y^+ > 20$). This change in the relative velocity occurs in the region where the particle relaxation time is of the same order of magnitude as the characteristic time of energy-containing eddies (Stokes number close to 1), so that particles respond slowly to changes of the local fluid velocity. Moreover, in the same region the interaction of particles with the sweep–burst cycle takes place; for $y^+ > 20$, particles are convected and lifted up by intense fluid ejections (bursts) carrying low-momentum fluid from the wall region (thus exhibiting a lower velocity in comparison to the surrounding fluid), whereas close to the wall ($y^+ < 20$) fluid injections (sweeps) carry along the wall high-momentum particles (which retain their velocity which is higher than that of the surrounding fluid).

The analysis of the profiles of the r.m.s. fluctuations of the streamwise and vertical velocity components shows that they are damped in the outer layer (especially for the vertical component) but enhanced in the inner region in comparison to the clear-water measurements. The results in the outer layer are different from what would be expected for a rough wall, where the r.m.s. fluctuations are observed to increase over the whole layer; therefore, the mechanism of particle–fluid interaction must be different from a simple increased equivalent wall roughness due to particles. Moreover, in the experiments with particle-laden conditions, the streamwise r.m.s. velocity of the solid phase is consistently larger than that of the fluid all along the measured vertical profile. On the other hand, the vertical fluctuations of the solid phase are larger than those produced by the fluid in the outer layer but smaller in the region $y^+ < 30$. The momentum balance in the vertical direction reveals a significant momentum exchange between the two phases, particularly effective in the buffer region where

https://doi.org/10.1017/S0022112004008304 Published online by Cambridge University Press

bursts are intense; the present measurements reveal that this momentum transfer is predominant in the vertical direction. This exchange leads to a reduction of the turbulent energy production in the buffer region which is no longer available for the turbulent diffusion processes in the outer layer. This mechanism could, at least in part, explain the turbulent damping observed in the outer layer. These considerations are clarified by considering the dynamics of the near-wall structures which make a connection between the behaviours in the buffer and outer regions ($y^+ > 20$) and those in the very near-wall region. In particle-laden conditions, for $y^+ > 20$, particles are lifted up by bursts, gain momentum from the fluid phase and carry fluctuations levels which are higher than those of the surrounding fluid (but still lower than in clear water). For $y^+ < 20$ sweeps carry particles with high r.m.s. velocities close to the wall and the observed fluctuations are even larger than in clear water. Under the last condition, the difference between particle and fluid fluctuations also depends on the presence of the wall which bounds the vertical fluctuations of the particles.

The previous picture is confirmed by the analysis of the Reynolds stress profiles; in comparison to the clear-water conditions, close to the wall there is an increment of the Reynolds stress (due to the particles moving from the high Reynolds stress region and preserving their motion due to inertia) and far from the wall there is a reduction (due to the fact that particles rapidly follow changes in fluid motion).

The question of particle–flow interaction is lastly addressed by separating the Reynolds stress intensity in 'coherent' or 'incoherent' events using the quadrant analysis. For 'coherent' events, the second quadrant corresponds to ejections, and the fourth to sweeps; first and third quadrant events are referred as 'incoherent'. The quadrant analysis indicates substantial differences in particle–fluid interactions between the wall ($y^+ < 10$) and the buffer regions. For $y^+ < 10$, the intensity of ejection events (second quadrant) gains importance over sweeps in sediment-laden conditions (in comparison to clear-water). On the other hand, in the buffer region both Reynolds stress coherent intensities decrease when comparing sediment-laden to clear-water conditions, the damping of ejection events being stronger than that of sweeps; this circumstance corroborates the previously mentioned hypothesis of a significant momentum transfer between the two phases. On average, burst and sweep intensities in particle-laden conditions have almost the same importance thus reflecting a higher degree of dynamical balance of the burst–sweep cycle when solid particles are present in comparison to clear water.

These results indicate that, at the particle concentrations used in the present measurements, particles significantly affect the flow field, not only in the outer part of the wall layer (as already reported by other authors), but mainly in the inner region, where particle concentration and inertia (in respect to the fluid) are higher. If this is true, the time sequence of wall events must also be modified by the particles; this is one of the points which deserve further investigations.

The authors wish to thank the fruitful help, support and suggestions provided by Antonio Cenedese.

REFERENCES

Adrian, R. J., Meinhart, P. & Tomkins, C. D. 2000 Vortex organization in the outer region of the turbulent boundary layer. *J. Fluid Mech.* **422**, 1–54.

Alimonti, C., Cenedese, A. & Cioffi, F. 1988 Measurements of velocity, dimension and concentration of solid particles in air and water by phase difference methods. In *Proc.*

https://doi.org/10.1017/S0022112004008304 Published online by Cambridge University Press

6th Intl Congr. on Optical Methods in Flow and Particle Diagnostics ICALEO '87 (ed. W. H. Stevenson), vol. 63, pp. 160–173. Laser Institute of America, Toledo (OH) USA.

Aubry, N., Holmes, P., Lumley, J. L. & Stone, E. 1988 The dynamics of coherent structures in the wall region of a turbulent boundary layer. *J. Fluid Mech.* **192**, 115–173.

Best, J., Bennett, S., Bridge, J. & Leeder, M. 1997 Turbulent modulation and particle velocities over flat sand beds at low transport rates. *J. Hydr. Engng ASCE* **123**, 1118–1129.

Bouvard, M. & Petkovic, S. 1985 Vertical dispersion of spherical, heavy particles in turbulent open channel flow. *J. Hydr. Res. IAHR* **23**, 5–20.

Buchhave, P., George, W. K. & Lumley, J. L. 1979 The measurement of turbulence with LDA. *Annu. Rev. Fluid Mech.* **11**, 443–503.

Cellino, M. & Graf, W. H. 1999 Sediment-laden flow in open channels under noncapacity and capacity conditions. *J. Hydr. Engng ASCE* **125**, 455–462.

Cenedese, A., Cioffi, F. & Romano, G. P. 1989 Doppler signal predictions using the Lorenz-Mie theory for applications to measurements in two-phase flows. *Arch. Mech.* **41**, 821–835.

Cioffi, F. & Gallerano, F. 1991 Velocity and concentration profiles of solid particles in a channel with a movable and erodible bed. *J. Hydr. Res. IAHR* **29**, 387–401.

Coleman, N. L. 1981 Velocity profiles with suspended sediment. *J. Hydr. Res. IAHR* **19**, 211–229.

Coleman, N. L. 1986 Effect of suspended sediment on the open channel velocity distribution. *Water Resour. Res.* **22**, 1377–1384.

Coles, D. 1956 The law of the wake in the turbulent boundary layer. *J. Fluid Mech.* **1**, 191–226.

Coles, D. E. 1968 The young person's guide to the data. In *Proc. AFOSR–IFP Stanford Conf. on Computation of Turbulent Boundary Layers, 1968* (ed. D. Coles & E. A. Hirst), vol. 2, pp. 1–45. Stanford University.

Durst, F., Melling, A. & Whitelaw, J. H. 1976 *Principle and Practise of LASER-Doppler Anemometry*. Academic.

Elgobashi, S. 1994 On predicting particle-laden turbulent flows. *Appl. Sci. Res.* **52**, 309–329.

Gore, R. & Crowe, C. T. 1989 Effect of particle size on modulating turbulence intensity. *Intl J. Multiphase flow* **15**, 279–285.

Graf, W. H. & Cellino, M. 1999 Turbulence suppression in suspension flow. In *Proc. XXVIII IAHR Congress, Theme D* (ed. G. Jirka & B. Manoha). Inst. Hydr. and Hydrol., Tech. Univ. of Graz, Graz, Austria.

Grass, A. J. 1974 Transport of fine sand on a flat bed: turbulence and suspension mechanics. In *Proc. Euromech 48, Inst. Hydrodynamic and Hydraulic Engng, Tech. Univ. of Denmark*, pp. 33–34.

Greimann, B. P., Muste, M. & Holly, F. M. 1999 Two-phase formulation of suspended sediment transport. *J. Hydr. Res. IAHR* **37**, 479–500.

Harder, K. J. & Tiederman, W. G. 1991 Drag reduction and turbulent structure in two-dimensional channel flows. *Phil. Trans. R. Soc. Lond.* A **336**, 19–34.

Hussain, A. K. M. F. 1986 Coherent structures and turbulence. *J. Fluid Mech.* **173**, 303–356.

Ishii, M. 1975 *Thermo-Fluid Dynamic Theory of Two-phase Flow*. Eyrolles, EDF, Paris.

Itakura, T. & Kishi, T. 1980 Open channel flow with suspended sediments. *J. Hydr. Div. ASCE* **106**, 1325–1343.

Kaftori, D., Hetsroni, G. & Banerjee, S. 1995*a* Particle behaviour in the turbulent boundary layer. I. Motion, deposition and entrainment. *Phys. Fluids* **7**, 1095–1106.

Kaftori, D., Hetsroni, G. & Banerjee, S. 1995*b* Particle behaviour in the turbulent boundary layer. II. Velocity and distribution profiles. *Phys. Fluids* **7**, 1107–1121.

Karlsson, R. J. & Johansson, T. G. 1986 In *Selected Papers of the 3rd Symp. on Application of Laser Techniques to Fluid Mechanics* (ed R. Adrian, D. F. G. Durao, F. Durst *et al.*), pp. 273–289. Springer.

Kim, H. T., Kline, S. J. & Reynolds, W. C. 1971 The production of turbulence near a smooth wall in a turbulent boundary layer. *J. Fluid Mech.* **50**, 133–160.

Kline, S. J., Reynolds, W. C., Schraub, F. A. & Runstadler, P. W. 1967 The structure of turbulent boundary layers. *J. Fluid Mech.* **30**, 741–773.

Krogstad, P. A. & Antonia, R. A. 1999 Surface roughness effects in turbulent boundary layers. *Exps. Fluids* **27**, 450–460.

Kulick, J. D., Fessler, J. R. & Eaton, J. K. 1994 Particle response and turbulence modification in fully developed channel flow. *J. Fluid Mech.* **277**, 109–134.

https://doi.org/10.1017/S0022112004008304 Published online by Cambridge University Press

Laufer, J. 1950 Investigation of turbulent flow in a two-dimensional channel. *NACA Tech. Note* TN2123.

Lu, S. S. & Willmarth, W. W. 1973 Measurement of structure of the Reynolds stress in a turbulent boundary layer. *J. Fluid Mech.* **60**, 481–511.

Lumley, J. L. 1978 Two-Phase and Non Newtonian Flows. In *Turbulence* (edited by P. Bradshaw), pp. 289–324. Springer.

Lyn, D. A. 1986 Turbulence and turbulent transport in sediment-laden open channel flows. *Rep.* KH-R-49. W. M. Keck Lab. of Hydr. and Water Resour. California Inst. of Tech., Pasadena, USA.

Lyn, D. A. 1988 A similarity approach to turbulent sediment-laden flows in open channels. Turbulence and turbulent transport in sediment-laden open channel. *J. Fluid Mech.* **193**, 1–26.

Muste, M. & Patel, V. C. 1997 Velocity profiles for particles and liquid in open-channel flow with suspended sediment. *J. Hydr. Engng. ASCE* **123**, 742–751.

Nakagawa, H. & Nezu, I. 1977 Prediction of the contribution to the Reynolds stress from the bursting events in open-channel flows. *J. Fluid Mech.* **80**, 99–128.

Nezu, I. & Nakagawa, H. 1993 *Turbulence in Open Channel Flows.* IAHR Monograph, A. A. Balkema.

Nezu, I. & Rodi, W. 1986 Open-channel flow measurements with a laser Doppler anemometer. *J. Hydr. Engng. ASCE* **112**, 335–355.

Niño, Y. & Garcia, M. H. 1996 Experiments on particle-turbulence interactions in the near-wall region of an open channel flow: implications for sediment transport. *J. Fluid Mech.* **326**, 285–319.

Owen, P. R. 1969 Pneumatic transport. *J. Fluid Mech.* **39**, 407–432.

Pedinotti, S., Mariotti, G. & Banerjee, S. 1992 Direct numerical simulation of particle behaviour in the wall region of turbulent flows in horizontal channels. *Intl J. Multiphase Flow* **18**, 927–941.

Rashidi, M., Hetsroni, G. & Banerjee, S. 1990 Particle-turbulence interaction in a boundary layer. *Intl J. Multiphase Flow* **16**, 935–949.

Righetti, M. 1994 Interaction between fluid and suspended sediments in the near-wall region of an open channel flow (in italian). PhD Thesis, University of Padova, Italy.

Rizk, M. & Elgobashi, S. E. 1985 The motion of a spherical particle suspended in a turbulent flow near a plane wall. *Phys. Fluids* A **3**, 928–937.

Robinson, S. K. 1991 Coherent motions in the turbulent boundary layer. *Annu. Rev. Fluid Mech.* **23**, 601–639.

Saffman, M. & Buchhave, P. 1984 Simultaneous measurement of size, concentration and velocity of spherical particles by a laser Doppler method. In *Proc. 2nd Symp. on Application of Laser Techniques to Fluid Mechanics* (ed. D. F. G. Durao), pp. 1–8. Ladoan, Lisbon, Portugal.

Shen, C. & Lemmin, U. 1999 Application of an acoustic particle flux profiler in particle-laden open-channel flow. *J. Hydr. Res. IAHR* **37**, 407–419.

Sumer, M. B. & Deigaard, R. 1981 Lift forces on moving particles near boundaries. Part 2. *J. Fluid Mech.* **109**, 311–337.

Sumer, M. B. & Oguz, B. 1978 Particle motions near the bottom in turbulent flow in an open channel. *J. Fluid Mech.* **86**, 109–127.

Tennekes, H. & Lumley, J. L. 1972 *A First Course in Turbulence*. MIT Press.

Tsuji, Y. & Morikawa, Y. 1982 LDV measurements of an air-solid two-phase flow in a horizontal pipe. *J. Fluid Mech.* **120**, 385.

Tsuji, Y., Morikawa, Y. & Shiomi, H. 1984 LDV measurements of an air-solid two-phase flow in a vertical pipe. *J. Fluid Mech.* **139**, 417–434.

Valiani, A. 1991 The von-Kàrmàn coefficient in sediment-laden flow. *J. Hydr. Res. IAHR* **29**, 129–136.

Vanoni, V. A. 1946 Transportation of suspended sediment by water. *Trans.* ASCE 111, Paper 2267, pp. 67–133.

Van Rijn, L. 1989 Handbook sediment transport by currents and waves. *Rep. H461.* Delft Hydraulics, The Netherlands.

Wei, T. & Willmarth, W. W. 1989 Reynolds-number effects on the structure of a turbulent channel flow. *J. Fluid Mech.* **204**, 57–96.

White, A. 1974 *Viscous Fluid Flow*. McGraw Hill.

Yalin, G. 1972 *Mechanics of Sediment Transport*. Pergamon.

https://doi.org/10.1017/S0022112004008304 Published online by Cambridge University Press